

Detecting hidden and composite orders in layered models via machine learning

W. Rzadkowski,¹ N. Defenu,² S. Chiacchiera,³ A. Trombettoni,^{4,5} and G. Bighin¹

¹*Institute of Science and Technology Austria (IST Austria), Am Campus 1, 3400 Klosterneuburg, Austria*

²*Institut für Theoretische Physik, Universität Heidelberg, D-69120 Heidelberg, Germany*

³*Science and Technology Facilities Council (STFC/UKRI), Daresbury Laboratory,*

Keckwick Lane, Daresbury, Warrington WA44AD, United Kingdom

⁴*CNR-IOM DEMOCRITOS Simulation Center, Via Bonomea 265, I-34136 Trieste, Italy*

⁵*SISSA and INFN, Sezione di Trieste, Via Bonomea 265, I-34136 Trieste, Italy*

(Dated: April 21, 2022)

We use machine learning to study layered spin models where composite order parameters may emerge as a consequence of the interlayerer coupling. We focus on the layered Ising and Ashkin-Teller models, determining their phase diagram via the application of a machine learning algorithm to the Monte Carlo data. Remarkably our technique is able to correctly characterize all the system phases also in the case of hidden order parameters, *i.e.* order parameters whose expression in terms of the microscopic configurations would require additional preprocessing of the data fed to the algorithm. Within the approach we introduce, owing to the construction of convolutional neural networks, naturally suitable for layered image-like data with arbitrary number of layers, no preprocessing of the Monte Carlo data is needed, also with regard to its spatial structure. The physical meaning of our results is discussed and compared with analytical data, where available. Yet, the method can be used without any *a priori* knowledge of the phases one seeks to find.

I. INTRODUCTION

Classification of observations into separate categories is certainly one of the most important applications of machine learning [1]. Successful examples range broadly from the detection of exotic particles in experimental high energy physics [2] through learning human actions in movies [3] to dermatologist-grade skin cancer classification [4]. The classification task is very often performed with artificial neural networks, capable of learning even highly complex and elusive patterns in the data, both detectable and invisible to humans. If multilayer image data is in question, convolutional neural networks (CNNs) perform exceptionally well, mimicking human vision by inferring from small portions of the image at a time. The CNNs have reached 99.77% accuracy [5] on the famous and highly competitive MNIST dataset [6] of hand-written digits.

Translational invariance and adjustable size of the filters, which detect local correlations, make CNNs the ideal candidates for phase diagram reconstruction. The phase diagram is typically reconstructed from a large number of Monte Carlo (MC) snapshots. At first, research efforts revolved around supervised learning on the MC snapshots [7–15], later shifting to fully unsupervised learning on a chosen observable, such as non-local correlators whose behaviour is modified by the presence of phase transitions [16].

In this paper we introduce a CNN-based approach capable of fully unsupervised learning of phase diagrams with the network fed exclusively with raw MC snapshots without any *a priori* knowledge about relevant observables or order parameters. We note that complementary approaches to the unsupervised learning problem have been pursued using principal component analysis and support vector machines [17–21], deep autoencoders [22] or discriminative cooperative networks [23]. However, here we show that the task of fully-unsupervised phase diagram reconstruction can also be performed using CNNs, allowing one to apply to physical prob-

lems a number of techniques developed in the field of computer vision, a field in which CNNs represents the golden standard.

Our approach is applied to the reconstruction of the phase diagram of layered spin models. Our motivation for such an investigation is three-fold. From one side, when two or more models are coupled, new phases can emerge as a result of the presence and of the form of the coupling, as it occurs in coupled spin systems. As an example, consider two critical magnetic systems with a tunable coupling between each other. When the coupling is zero, each system separately undergoes a conventional ferromagnetic phase transition [24]. For finite coupling, on the other hand, the order parameter will most likely involve some non-trivial combination of spins of both systems.

A paradigmatic example of such behavior is given by the so-called Ashkin-Teller model, where two square-lattice Ising models with spin variables $\sigma_i = \pm 1$ and $\tau_i = \pm 1$ (in layers 1 and 2, respectively) are coupled via a term of the form $\sigma\sigma\tau\tau$ [25, 26]. When this interlayer coupling is zero, the phase diagram of the model is characterized by the order parameters $\langle\sigma\rangle$ and $\langle\tau\rangle$. On the other hand, when the interlayer coupling is large enough with respect to the intralayer term, a new non-trivial phase with a composite order parameter $\langle\sigma\tau\rangle$ emerges. Since the phase diagram of the 2D Ashkin-Teller model and of some its variations can be determined analytically [26, 27], it provides an ideal benchmark to look for composite order parameters in an unsupervised way. Although in the two-variable (or, in our language, bi-layer) Ashkin-Teller model the composite order parameter can be easily recognized, a more complex spin model with several layers, with both short- and long-range interlayer couplings, could be much more challenging to be addressed with simple physical considerations. Many, possibly competing, composite order parameters may be present and determining the one which actually breaks the symmetry and generates a novel phase is a non-trivial task. To give an example of this difficulty we may

consider the case in which more Ising models are coupled in various ways, as the trilayer Ising model studied below. From this point of view, an unsupervised approach able to correctly reproduce the phase diagram of layered models, regardless of the nature of underlying order parameters, is highly desirable.

Our second motivation is that layered models emerge in a wide range of physical situations. Among them, the bilayer structure in which two two-dimensional systems are coupled has been studied in a number of cases, ranging from graphene [28] to quantum Hall systems [29] and ultracold dipolar gases [30]. Another major example is provided by layered superconductors, that can occur naturally or be artificially created. Among the former class, of primary importance are compounds of transition-metal dichalcogenides layers intercalated with organic molecules [31] and cuprates [32]. In cuprates, the layered structure is due to the presence of intercalant elements and a charge reservoir unit among CuO_2 planes. Examples of artificial structures are alternating layers of graphite and alkali metals [33] or samples with layers of different metals [34]. Neutral layered superfluids can be engineered with quantum gases by using a deep optical lattice in one spatial direction with ultracold fermions [35] or bosons [36]. Given the importance of layered physical systems in a variety of contexts, a general approach to individuate their phase diagram would provide an important tool of investigation.

Finally, our last motivation is purely methodological and internal to machine learning. Indeed, in layered models one has a certain degree of arbitrariness in the way the MC data to be analyzed are fed to the neural networks, *e.g.* one can provide the data in each layer separately, or retaining their spatial structure such as columns and ordering them correspondingly. As an example, in the Ashkin-Teller model one can provide numerical algorithms either with all the σ_i 's and then all the τ_i 's, or the pairs (σ_i, τ_i) according to the index i labeling the position of the spins in the layers. This arbitrariness also reflects itself in the fact that an order parameter which can be clearly identified with a choice can be non-trivial, or “hidden”, with another choice. To use again the Ashkin-Teller model as an example, the order parameter $\langle \sigma \tau \rangle$ is immediately identified when the choice of the pairs (σ_i, τ_i) is done, but not when the data are given by layers. Therefore a natural question is how to identify phase transitions in coupled or layered models driven by order parameters which may be hidden by the codification of the data to be provided to the machine learning algorithm.

II. MACHINE LEARNING PHASE TRANSITIONS IN CLASSICAL SPIN MODELS

Let us consider a general case of a spin system whose Hamiltonian is defined by two parameters, J and K . We aim to devise a procedure to depict the phase diagram in the $K - J$ plane. To this extent we discretize a portion of the $K - J$ plane on a grid with steps ΔJ and ΔK . For each point on the grid we generate a number of uncorrelated MC snapshots using standard algorithms [37–39]. Unless otherwise specified we shall work on a $32 \times 32 \times N_l$ square lattice, N_l being the number of

layers to be specified later, and we shall generate a number of 600 snapshots for each point in the phase diagram.

The training of the convolutional neural network attempts at learning to distinguish snapshots belonging to the two different points, (J_1, K_1) and (J_2, K_2) , in the phase diagram. Intuitively, when this training fails, the two points present nearly identical features, thus belonging to the same phase. On the other hand, if it succeeds, the two points should belong to two different phases. In order to carry out this plan, at first, we divide the data in a standard way, taking 80% of snapshots as training data, while keeping the other 20% as validation data. Then, we train the network on the training data and quantify the classification accuracy on the validation set as the fraction φ of correctly labeled examples from the validation set. Based on that, we introduce the following quasidistance [81] between the two phase diagram points (J_1, K_1) and (J_2, K_2) :

$$d((J_1, K_1), (J_2, K_2)) = 2(\varphi - 0.5)\Theta(\varphi - 0.5), \quad (1)$$

where $\Theta(x)$ is the Heavyside step function, preventing d from assuming negative values. Then perfect discrimination $\varphi = 1$ (signaling different phases) corresponds to $d = 1$, while perfect confusion $\varphi = 0.5$ (signaling the same phase) corresponds to $d = 0$.

We feed the raw Monte Carlo snapshots directly to the convolutional neural network, with spin down encoded as 0 and spin up encoded as 1, no preprocessing applied. The network architecture is optimized for the task of classifying two phases: after convolutional and fully connected layers the final layer consists of two softmax output neurons outputting the labels. Further technical details on the network architecture and training can be found in the Appendix.

At last, we make use of the distances defined in Eq. (1) to construct a field $u(J, K)$ defined on the phase diagram through its finite-difference lattice gradient

$$\begin{aligned} \nabla u(J, K) &= \begin{pmatrix} (u(J + \Delta J, K) - u(J, K)) / \Delta J \\ (u(J, K + \Delta K) - u(J, K)) / \Delta K \end{pmatrix} \equiv \\ &\equiv \begin{pmatrix} d((J + \Delta J, K), (J, K)) / \Delta J \\ d((J, K + \Delta K), (J, K)) / \Delta K \end{pmatrix}. \end{aligned} \quad (2)$$

Clearly ∇u will be constant in regions of the phase diagram belonging to the same phase, since we expect that the difficulty of telling first neighbors apart should be uniformly quite high. On the other hand, we expect the value of ∇u to abruptly change in the vicinity of a phase transition, suggesting that the phase diagram should be naturally characterized by looking at the finite-difference lattice Laplacian

$$\begin{aligned} \nabla^2 u(J, K) &\approx \frac{1}{(\Delta J)^2} \sum_{i=0}^N (-1)^i \binom{n}{i} u(J + (n/2 - i)\Delta J, K) + \\ &+ \frac{1}{(\Delta K)^2} \sum_{i=0}^N (-1)^i \binom{n}{i} u(J, K + (n/2 - i)\Delta K), \end{aligned} \quad (3)$$

with the $N = 2$, $N = 3$ and $N = 4$ cases corresponding to a 5-point, 9-point or 13-point stencil, respectively. The stencil includes $(N - 1)$ nearest neighbors in the J and K directions.

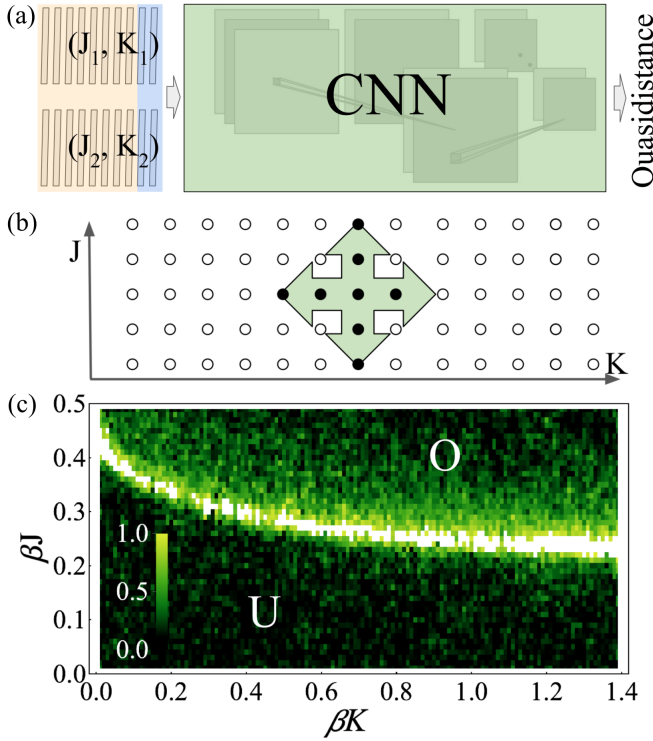


Figure 1: An overview of the proposed method. (a) The convolutional neural network is able to assess quasidistance which determines whether the phase diagram points (J_1, K_1) and (J_2, K_2) belong to the same or different phase. This is done by attempting to learn to distinguish between individual Monte Carlo snapshots with orange and blue visualizing training and validation MC snapshots, respectively, see main text. (b) Using distances between first, second and third neighbors, one can evaluate the Laplacian across the phase diagram. (c) Large values of the Laplacian signal the presence of phase transition. Plotting the Laplacian reconstructs the phase diagram, which is now parametrized by the adimensional combinations βJ and βK , with β the inverse temperature. Here we show the reconstructed phase diagram for the square-lattice Ising bilayer model, see main text.

We stress that the summations can be rearranged so that they involve only differences of the u field evaluated between first, second and third neighbors, that can in turn be expressed in terms of the quasidistance d . From the discussion above, it is clear that a sudden rise in the value of $\nabla^2 u$ means that the CNN can distinguish with increased precision arbitrarily close points in the phase diagram, thus signaling a phase transition. We anticipate that including high-order finite-differences besides the obvious 5-point stencil taking into account first-neighbors stencil considerably increases the quality of the reconstructed phase diagram. This point will be analyzed in detail later.

In conclusion of the present Section, we compare our scheme with other related approaches. As opposed to other machine learning schemes, in the present work we do not need the evaluation of any observable quantity to establish a distance [16], rather directly relying on the MC snapshots. Moreover, as opposed to other approaches [40] the scheme

we introduce in this paper fully takes advantage of the two-dimensional nature of a two-parameter phase diagram, as the local information is reconstructed by taking into account neighbours in all directions. Extensions to three- or higher-dimensional phase diagrams are straightforward [41]. Finally, our approach requires only the evaluation of a fixed number of neighbors for each point in the phase diagram, ensuring that the computational effort required for training scales linearly with the number of points in the discretized phase diagram.

III. MULTI-LAYER ISING MODELS

We now use the framework described in the previous Section to characterize the phase diagram of three different coupled spin models.

Let us start from a bilayer Ising system, described by the following Hamiltonian with a quadratic coupling term (sometimes referred to as the Yukawa coupling):

$$H_{\text{bilayer}} = -J \sum_{\langle ij \rangle} \sigma_i \sigma_j - J \sum_{\langle ij \rangle} \tau_i \tau_j - K \sum_i \sigma_i \tau_i, \quad (4)$$

where $\sigma_i, \tau_i = \pm 1$ are Ising variables on a two-dimensional square lattices, whose sites are denoted by the indices i, j . The sums in Eq. (4) are over nearest-neighbor sites. When $K = 0$, the system reduces to two uncoupled Ising models, having a phase transition at the Onsager critical point $(\beta J)_c = \ln(1 + \sqrt{2})/2$ [42, 43], β being the inverse temperature. This critical point is shifted by the presence of a finite interlayer coupling K . The resulting Ising critical line separating the paramagnetic and ferromagnetic phases as a function of K has been studied in the literature [44–46]. It is clear that the bilayer system (4) is the classical counterpart of two coupled quantum Ising chains in a transverse field, a system that has been studied both in relation to its spectrum, phase transitions and possibility to determine an integrable line in the space of parameters [47–50]. The classical bilayer system and the quantum coupled chains can be also related to each other by an exact mapping.

From our point of view the model described by Eq. (4) is an excellent starting point for our investigations, especially in order to check the existence of a composite order parameter and its relation to the phase diagram. It is now natural to parametrize the phase diagram in term of the dimensionless combinations βJ and βK , discretizing it for values of $\beta J \in [0, 0.5]$ and $\beta K \in [0, 1.4]$, with discretization steps $\Delta \beta J = \Delta \beta K = 0.01$. We then apply the phase diagram reconstruction procedure described in the previous Section to precisely determine the phase boundaries in the βK - βJ phase diagram, shown in Fig. 1(c). The phase transition occurs at $(\beta J)_c \approx 0.44$ in the uncoupled $\beta K = 0$ case, in agreement with analytical results [42, 43]. Then the critical temperature gradually decreases to the strong-coupling critical temperature $(\beta J)'_c = (\beta J)_c/2$. The width of the peak is essentially due to the finite-size ($32 \times 32 \times 2$) of the lattice used for Monte Carlo simulations, whose snapshots we feed to the neural network. The result is that it appears that only two phases are found, with order parameter $\langle \sigma \rangle = \langle \tau \rangle$. From our treatment of

data we cannot determine the behavior of the order parameter inside the two phases, whose study would be an interesting future continuation of the present results.

Next, we consider a trilayer system, whose Hamiltonian is a natural extension of the one of Eq. (4):

$$H_{\text{trilayer}} = -J \sum_{\langle ij \rangle} \sigma_i \sigma_j - J \sum_{\langle ij \rangle} \tau_i \tau_j - J \sum_{\langle ij \rangle} v_i v_j + \\ - K \sum_i \sigma_i \tau_i - K \sum_i \tau_i v_i, \quad (5)$$

and the new variable v_i is also an Ising spin. This is the first non-trivial example, and of course representative of properties of the multi-layer Ising model with Yukawa coupling. The central natural question is whether a composite order parameter emerges. Moreover the model of Eq. (5) is interesting since it paves the way to the investigation of the N layers case, which shall be trivial with the method presented here. Indeed the N layer case may serve to investigate how the (three-dimensional) limit of infinite layers is retrieved, an issue in the context of layered models, see *e.g.* [51].

The investigation of the model described by Eq. (5) follows the same line as the one of the bilayer case, we are able to reconstruct the phase diagram as shown in Fig. 2, recovering that strong-interlayer-coupling critical temperature that in this case is $(\beta J)_c'' = (\beta J)_c/3$, marked by a red dashed line. The main result exhibited in Fig. 2 is that no composite order parameter appears even for the trilayer case. Therefore, our technique has been able to correctly recover the phase diagram of the bilayer Ising model, where we do not expect any additional order to appear [52, 53], while it also predicts the same picture for the trilayer case, for which no previous expectation exist up to our knowledge. The generalization to the N -layer case shall be straightforward, but more numerically demanding, while based on the present results no additional phases are expected to appear. Therefore, in the following we are going to investigate a different case where a composite order parameter appears by construction.

IV. RECONSTRUCTING HIDDEN ORDER PARAMETERS: THE ASHKIN-TELLER MODEL

We now turn to the square-lattice Ashkin-Teller model, described by the following Hamiltonian

$$H_{\text{AT}} = -J \sum_{\langle ij \rangle} \sigma_i \sigma_j - J \sum_{\langle ij \rangle} \tau_i \tau_j - K \sum_{\langle ij \rangle} \sigma_i \sigma_j \tau_i \tau_j \quad (6)$$

with $\sigma_i, \tau_i = \pm 1$. Compared to Hamiltonians (4)-(5) one sees that the coupling is now quartic in spins. Since in the Ising model there are only two scaling fields relevant in renormalization group sense [24, 43], the magnetization and the energy, one sees that in the models (4) and (6) one has basically the two natural ways of having respectively magnetization-magnetization and energy-energy couplings, higher order coupling terms being irrelevant. The Ashkin-Teller model is also related to the four state planar Potts model, and several

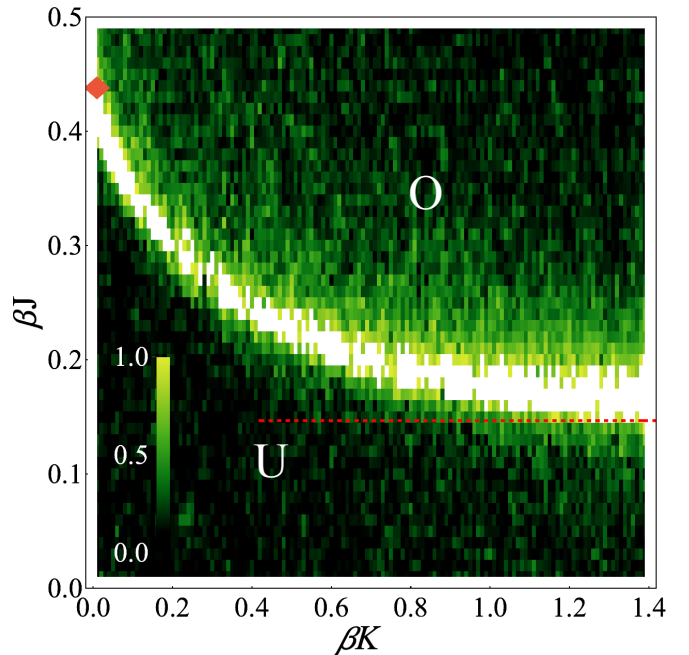


Figure 2: Reconstructed phase diagram for the square-lattice Ising trilayer model, showing a phase transition between an unordered, high-temperature phase (U) to an ordered, low-temperature phase (O). Note that as the interlayer interaction βK is increased, the critical temperature decreases from the analytic limit $(\beta J)_c = \ln(1 + \sqrt{2})/2 \approx 0.44$, marked by a red diamond, to the strong-interlayer-coupling limit $\beta K \rightarrow \infty$ where $(\beta J)'_c = (\beta J)_c/3$, marked by a red, dashed line.

variations of it, also in three dimensions, have been investigated [54].

The Ashkin-Teller model features a rich phase diagram, and remarkably in two dimensions can be studied analytically [26, 27]. Here we consider the case of ferromagnetic couplings, $J, K \geq 0$. It is known that three different phases exist [26]. Besides an ordered phase, denoted by I, characterized by $\langle \sigma \rangle \neq 0 \neq \langle \tau \rangle$ and a disordered phase, II, characterized by $\langle \sigma \rangle = \langle \tau \rangle = 0$ one also finds the peculiar phase III in which the single spins σ and τ are disordered, whereas a composite order parameter given by their product is ferromagnetically ordered, *i.e.* $\langle \sigma \tau \rangle \neq 0$.

Whereas the previous investigation of Ising-like models makes us confident that the ML procedure we have introduced is able to correctly characterize the transition between phase I and phase II, it is not *a priori* clear that phase III can be correctly identified. As shown in the small inset of Fig. 3, MC snapshots show disordered spins both in phase II and in phase III, the transition being determined by the $\sigma \tau$ composite variable, that we do not directly feed to the CNN. In order to learn the existence of the II-III phase transition the CNN must learn to reconstruct the composite order parameter. We find that our framework successfully performs this task, owing to the convolutional filters which are convolved in 2D spanning across the layers and are able to learn even elusive interlayer correlations.

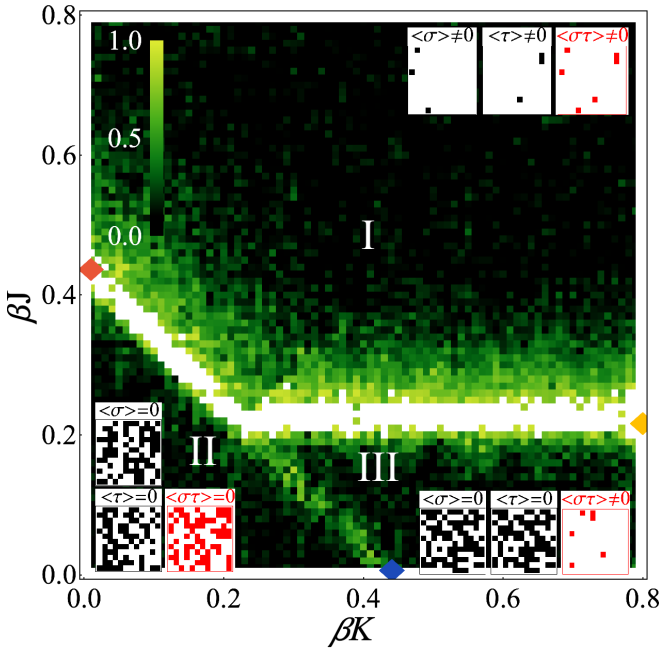


Figure 3: Reconstructed phase diagram for the square-lattice Ashkin-Teller model: the red, blue and yellow diamonds show analytically-determined phase transition points, see main text. Our approach identifies three phases, in agreement with the theory of the Ashkin-Teller model. The insets show representative configurations of the σ , τ spins and of the ‘composite’ spin $\sigma\tau$, for each phase: note that the transition between phase II and phase III does not correspond to any apparent difference in the σ and τ layers that we feed to the CNN. We stress that the $\sigma\tau$ ‘composite’ variable, marked in red, is not fed to the CNN.

The reconstructed phase diagram of Fig. 3 shows that indeed our approach is able to correctly learn the phase transitions in the ferromagnetic Ashkin-Teller model. Whereas the transition line corresponding to the magnetization of σ and τ , as separated variables, corresponds to a prominent peak, whose width is essentially determined by finite-size effects, the line corresponding to the magnetization of the composite $\sigma\tau$ order parameter corresponds to a smaller peak, displaying that the characterization of this transition line is more demanding to the CNN, but still possible.

We can compare the obtained phase diagram we obtain with some exact results. In the $K \rightarrow 0$ the model reduces to a square-lattice Ising model with coupling constant J , with critical temperature $(\beta J)_c = \ln(1 + \sqrt{2})/2 \approx 0.44$ [42, 43], whereas in the $K \rightarrow \infty$ limit the model reduces to a square-lattice Ising model with coupling constant $2J$ and critical temperature $(\beta J)'_c = \ln(1 + \sqrt{2})/4 \approx 0.22$. Finally for $J = 0$ the system again undergoes an Ising-like phase transition for the composite order parameter, at $(\beta K)_c = \ln(1 + \sqrt{2})/2 \approx 0.44$. These three points are marked by a red, yellow and blue diamond, respectively, in the phase diagram of Fig. 3, showing an excellent agreement between the analytical results and the reconstructed phase diagram, even in the latter case when the composite order parameter $\sigma\tau$ drives the transition.

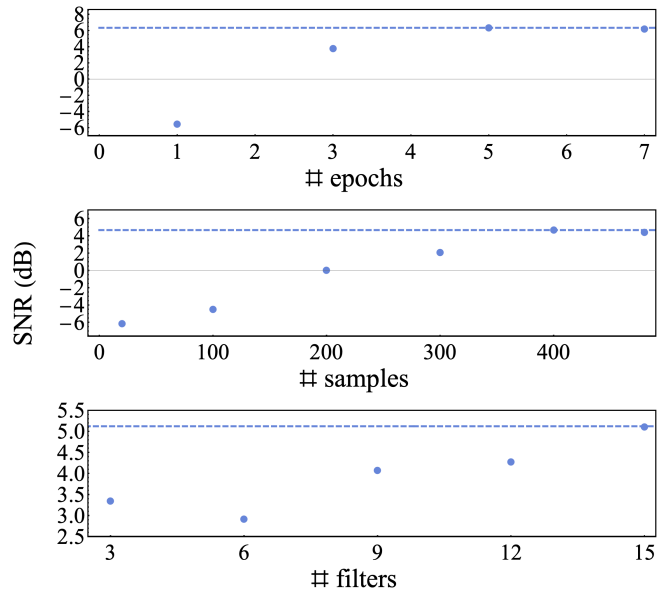


Figure 4: Signal-to-noise ratio as a function of the number of epochs (upper panel), of the number of samples in the training set (middle panel) and of the number of convolutional filters (lower panel). The dashed lines guide the eye towards the highest attainable signal-to-noise ratio in each dataset.

V. SCALING PROPERTIES AND ROBUSTNESS OF THE APPROACH

Our results show that with the network and learning parameters that we used we were able to obtain a phase diagram of quality high enough to visually identify different phases. In addition, in this Section we characterize our method by quantifying signal to noise ratio (SNR) and studying its behavior when essential parameters are changed. We define the SNR as

$$\text{SNR} \equiv \log_{10} \left(\frac{\frac{1}{N} \sum_i (x_i - \nu)^2}{\nu^2} \right), \quad (7)$$

x_i being the values of the $\nabla^2 u$ field of Eq. (3), the summation extending over a region containing N values, ν being the ‘noise’, i.e. the average value of $\nabla^2 u$ in a subset of the region far away from a phase transition. We evaluate the SNR for the Ising bilayer on a strip centered on $\beta K = 1.1$, exhibiting a sharp phase transition at $\beta J \approx 0.26$ as clear from Fig. 1. At first, we vary the number of training epochs, observing that the SNR is rapidly increasing before reaching a maximum value at around 5 epochs of training. This indicates that further training brings no benefit while providing a risk of overfitting, justifying our early-stopping approach. Secondly, we vary the number of samples in the training set, showing a rapid increase in the SNR before reaching a plateau at about 400 samples, justifying our choice of using a slightly larger number (600) of samples in the training set. Lastly, we vary the number of convolutional filters in the CNN. Again, the general upwards trend shows that a larger number of convolutional filters helps in enhancing the quality of the reconstructed phase diagrams. However, we stress that in this latter

case the SNR is quite high in the whole parameter region we consider. The lowest number of convolutional filters we consider (3) is already enough for achieving a good reconstruction of the phase diagram and a large SNR value. These analyses are shown in Fig. 4.

We have also analysed how the reconstructed phase transition is affected by the dimension of the stencil in Eq. (3). Using a 5-point, 9-point or 13-point stencil we have obtained SNR values of -1.36 dB, 0.38 dB and 3.88 dB, respectively. This confirms that the approach we are introducing takes indeed great advantage from the two-dimensional structure of the phase diagram, and information from second- and third-nearest neighbors is being used to sharply characterize the phase transition.

VI. CONCLUSIONS

Thus, as shown for layered spin models such as the multi-layer Ising and Ashkin-Teller models, our work demonstrates that ML approaches are able to learn the order parameter driving a phase transition in layered models, also when this parameter is not immediately apparent from the snapshots without preprocessing. This is directly possible due to the convolutional filters which are, without any *a priori* knowledge, capable of learning even involved algebraic operations that uncover the order parameters from the data. This paves the way to the use of ML approaches to investigate the properties of systems of increasing complexity and to characterizing phases of matter described by multiple, possibly non-local order parameters, the universal approximation theorem [55] ensuring that a neural network can, at least in principle, learn to recognize arbitrarily complex order parameters. In particular it would be very interesting to study the multi-layer Ising model with a number of layers increasing, the three-dimensional Ashkin-Teller and the trilayer Ahkin-Teller in two dimensions, which can be studied with the techniques introduced in the paper. Non-local couplings among the layers could be added, which would lead to non-local, more composite, operators. These results should be compared with the identification of hidden order done using non-ML techniques [56]. Also, the present approach may be used for other cases in which the identification of the order parameters is not straightforward [57–59].

Naturally, the approach we introduced could also be used to characterize quantum models, or classical spin models with competition between short- and long-range interactions. We

expect that by an appropriate choice of the sizes and strides of the filter in the convolutional layer one could characterize antiferromagnetic order parameters, non-local order parameters and exotic order parameters, such as nematic and smectic phases. In this context, current experiments on fermionic dipolar atoms [60, 61] promise to open a new window in the physics of competing long-range and short-range interactions [62], clearing the path for the comprehension of modulated phases in strongly interacting quantum systems.

The presence of spatially ordered structures is a *leitmotiv* for long-range and layered systems such as ultra-thin magnetic films [63–65], iron-based superconductors and cuprates [66, 67]. The pattern structure normally depends on several experimental conditions and it produces a particularly rich phase diagram. Most of the common features occurring in stripe forming systems and modulated phases remain obscure due to the challenges posed by the complicated order parameters, which occur in these cases [68–71]. The ML technique introduced in the present paper may serve as an essential prove to finally uncover the complexity of such phases.

Our results pave the way for fully automated study of phase diagrams of more general and complicated spin systems. An exciting open problem lying in the realm of so-called explainable artificial intelligence (XAI) [72] is whether machine learning techniques could not only learn to separate phases differing by a ‘hidden’ order parameter, but also identify that parameter. Another natural development of the present work is to use our fully-unsupervised technique to learn directly from experimental data [73, 74]. Finally, it would be interesting to extend the results presented in this paper according the variational procedure discussed in [75].

Acknowledgments

We thank Gesualdo Delfino, Michele Fabrizio, Piero Ferrarese, Robert Konik, Christoph Lampert and Mikhail Lemeshko for stimulating discussions at various stages of this work. W.R. has received funding from the EU Horizon 2020 programme under the Marie Skłodowska-Curie Grant Agreement No. 665385. G.B. acknowledges support from the Austrian Science Fund (FWF), under project No. M2461-N27. N.D. acknowledges support by the Deutsche Forschungsgemeinschaft (DFG) via Collaborative Research Centre SFB 1225 (ISOQUANT) and under Germany’s Excellence Strategy EXC-2181/1-390900948 (Heidelberg STRUCTURES Excellence Cluster).

[1] G. Carleo, I. Cirac, K. Cranmer, L. Daudet, M. Schuld, N. Tishby, L. Vogt-Maranto, and L. Zdeborová, arXiv.org (2019).
[2] P. Baldi, P. Sadowski, and D. Whiteson, *Nature communications* **5**, 4308 (2014).
[3] I. Laptev, M. Marszałek, C. Schmid, and B. Rozenfeld, in *CVPR 2008-IEEE Conference on Computer Vision & Pattern Recognition* (IEEE Computer Society, 2008), pp. 1–8.
[4] A. Esteva, B. Kuprel, R. A. Novoa, J. Ko, S. M. Swetter, H. M. Blau, and S. Thrun, *Nature* **542**, 115 (2017).
[5] D. Cireşan, U. Meier, and J. Schmidhuber, arXiv preprint arXiv:1202.2745 (2012).
[6] Y. LeCun, <http://yann.lecun.com/exdb/mnist/> (1998).
[7] J. Carrasquilla and R. G. Melko, *Nature Physics* **13**, 431 (2017).
[8] E. P. L. van Nieuwenburg, Y.-H. Liu, and S. D. Huber, *Nature Physics* **13**, 435 (2017).

[9] D. Kim and D.-H. Kim, Phys. Rev. E **98**, 022138 (2018).

[10] C. Casert, T. Vieijra, J. Nys, and J. Ryckebusch, Phys. Rev. E **99**, 023304 (2019).

[11] X. L. Zhao and L. B. Fu, arXiv.org (2018).

[12] Richter-Laskowska, Khan, Trivedi, and Maśka, Condensed Matter Physics **21**, 33602 (2018).

[13] X.-Y. Dong, F. Pollmann, and X.-F. Zhang, Phys. Rev. B **99**, 26 (2019).

[14] R. Zhang, B. Wei, D. Zhang, J.-J. Zhu, and K. Chang, Phys. Rev. B **99**, 821 (2019).

[15] M. J. S. Beach, A. Golubeva, and R. G. Melko, Phys. Rev. B **97**, 045207 (2018).

[16] P. Broecker, F. F. Assaad, and S. Trebst, arXiv.org (2017).

[17] R. Jadrich, B. Lindquist, and T. Truskett, J. Chem. Phys. **149**, 194109 (2018).

[18] R. Jadrich, B. Lindquist, W. Piñeros, D. Banerjee, and T. Truskett, J. Chem. Phys. **149**, 194110 (2018).

[19] W. Badawi, Z. Osman, M. Sharkas, and M. Tamazin, in *2017 Progress In Electromagnetics Research Symposium-Spring (PIERS)* (IEEE, 2017), pp. 326–331.

[20] P. Ponte and R. G. Melko, Phys. Rev. B **96**, 205146 (2017).

[21] R. Woloshyn, arXiv preprint arXiv:1905.08220 (2019).

[22] C. Alexandrou, A. Athenodorou, C. Chrysostomou, and S. Paul, arXiv preprint arXiv:1903.03506 (2019).

[23] Y.-H. Liu and E. P. L. van Nieuwenburg, Phys. Rev. Lett. **120**, 176401 (2018).

[24] J. Cardy, *Scaling and renormalization in statistical physics* (1996).

[25] J. Ashkin and E. Teller, Phys. Rev. **64**, 178 (1943).

[26] R. J. Baxter, *Exactly Solved Models in Statistical Mechanics*, Dover books on physics (Dover Publications, 2007).

[27] G. Delfino and P. Grinza, Nuclear Physics B **682**, 521 (2004), ISSN 0550-3213.

[28] K. S. Novoselov, A. K. Geim, S. V. Morozov, D. Jiang, Y. Zhang, S. V. Dubonos, I. V. Grigorieva, and A. A. Firsov, Science **306**, 666 (2004), ISSN 0036-8075.

[29] J. Jain, *Composite fermions* (2007).

[30] M. A. Baranov, M. Dalmonte, G. Pupillo, and P. Zoller, Chemical Reviews **112**, 5012 (2012).

[31] F. R. Gamble, F. J. DiSalvo, R. A. Klemm, and T. H. Geballe, Science **168**, 568 (1970), ISSN 0036-8075.

[32] M. Tinkham, *Introduction to Superconductivity* (1996).

[33] N. B. Hannay, T. H. Geballe, B. T. Matthias, K. Andres, P. Schmidt, and D. MacNair, Phys. Rev. Lett. **14**, 225 (1965).

[34] S. T. Ruggiero, T. W. Barbee, and M. R. Beasley, Phys. Rev. Lett. **45**, 1299 (1980).

[35] Iazzi, M., Fantoni, S., and Trombettoni, A., EPL (????).

[36] M. A. Cazalilla, A. Iucci, and T. Giamarchi, Phys. Rev. A **75**, 051603 (2007).

[37] R. H. Swendsen and J. S. Wang, Phys. Rev. Lett. **58**, 86 (1987).

[38] J. Salas and A. D. Sokal, Journal of Statistical Physics **85**, 297 (1996).

[39] U. Wolff, Phys. Rev. Lett. **62**, 361 (1989).

[40] P. Broecker, F. F. Assaad, and S. Trebst, arXiv.org (2017).

[41] S. P. Thampi, S. Asumali, R. Adhikari, and S. Succi, Journal of Computational Physics **234**, 1 (2013).

[42] L. Onsager, Phys. Rev. **65**, 117 (1944).

[43] G. Mussardo, *Statistical field theory: an introduction to exactly solved models in statistical physics* (2010).

[44] J. Oitmaa and I. G. Enting, Journal of Physics A: Mathematical and General **8**, 1097 (1975).

[45] P. L. Hansen, J. Lemmich, J. H. Ipsen, and O. G. Mouritsen, Journal of Statistical Physics **73**, 723 (1993), ISSN 1572-9613.

[46] R. Brower, K. Orginos, Y. Shen, and C.-I. Tan, Physica A: Statistical Mechanics and its Applications **221**, 554 (1995), ISSN 0378-4371.

[47] G. Delfino and G. Mussardo, Nuclear Physics B **516**, 675 (1998), ISSN 0550-3213.

[48] M. Fabrizio, A. Gogolin, and A. Nersesyan, Nuclear Physics B **580**, 647 (2000), ISSN 0550-3213.

[49] A. M. Tsvelik, *Quantum field theory in condensed matter physics* (Cambridge university press, 2007).

[50] R. M. Konik and Y. Adamov, Phys. Rev. Lett. **102**, 097203 (2009).

[51] T. Schneider and J. Singer, *Phase transition approach to high temperature superconductivity* (1998).

[52] J. Smiseth, E. Smørgrav, E. Babaev, and A. Sudbø, Phys. Rev. B **71**, 12 (2005).

[53] K. A. H. Sellin and E. Babaev, Phys. Rev. B **93**, 503 (2016).

[54] F. Y. Wu, Rev. Mod. Phys. **54**, 235 (1982).

[55] K. Hornik, Neural Networks **4**, 251 (1991).

[56] S. Martiniani, P. M. Chaikin, and D. Levine, Phys. Rev. X **9**, 011031 (2019).

[57] S. C. Riggs, M. C. Shapiro, A. V. Maharaj, S. Raghu, E. D. Bauer, R. E. Baumbach, P. Giraldo-Gallo, M. Wartenbe, and I. R. Fisher, Nature Communications **6**, 2727 (2015).

[58] M. H. Lee, C. P. Chang, F. T. Huang, G. Y. Guo, B. Gao, C. H. Chen, S. W. Cheong, and M. W. Chu, Phys. Rev. Lett. **119**, 157601 (2017).

[59] C. M. Varma and L. Zhu, Phys. Rev. Lett. **96**, 1265 (2006).

[60] M. Lu, N. Q. Burdick, and B. L. Lev, Phys. Rev. Lett. **108**, 215301 (2012).

[61] J. W. Park, S. A. Will, and M. W. Zwierlein, Phys. Rev. Lett. **114**, 205302 (2015).

[62] S. Baier, D. Petter, J. H. Becher, A. Patscheider, G. Natale, L. Chomaz, M. J. Mark, and F. Ferlaino, Phys. Rev. Lett. **121**, 093602 (2018).

[63] R. Allenspach and A. Bischof, Phys. Rev. Lett. **69**, 3385 (1992).

[64] A. Kashuba and V. L. Pokrovsky, Phys. Rev. Lett. **70**, 3155 (1993).

[65] A. B. Kashuba and V. L. Pokrovsky, Phys. Rev. B **48**, 10335 (1993).

[66] C. V. Parker, P. Aynajian, E. H. da Silva Neto, A. Pushp, S. Ono, J. Wen, Z. Xu, G. Gu, and A. Yazdani, Nature **468**, 677 (2010).

[67] M. A. Tanatar, A. E. Böhmer, E. I. Timmons, M. Schütt, G. Drachuck, V. Taufour, K. Kothapalli, A. Kreyssig, S. L. Bud'ko, P. C. Canfield, et al., Phys. Rev. Lett. **117**, 127001 (2016).

[68] A. Mendoza-Coto, D. G. Barci, and D. A. Stariolo, Phys. Rev. B **95**, 175 (2017).

[69] A. Mendoza-Coto and D. A. Stariolo, Phys. Rev. E **86**, 85 (2012).

[70] D. G. Barci and D. A. Stariolo, Phys. Rev. B **79**, 85 (2009).

[71] D. G. Barci and D. A. Stariolo, Phys. Rev. B **84**, 175 (2011).

[72] F. K. Došilović, M. Brčić, and N. Hlupić, in *2018 41st International convention on information and communication technology, electronics and microelectronics (MIPRO)* (IEEE, 2018), pp. 0210–0215.

[73] A. Bohrdt, C. S. Chiu, G. Ji, M. Xu, D. Greif, M. Greiner, E. Demler, F. Grusdt, and M. Knap, arXiv.org (2018).

[74] Y. Zhang, A. Mesaros, K. Fujita, S. D. Edkins, M. H. Hamidian, K. Ch'ng, H. Eisaki, S. Uchida, J. C. S. Davis, E. Khatami, et al., arXiv.org (2018).

[75] M. Koch-Janusz and Z. Ringel, Nature Physics **14**, 578 (2018).

[76] D. Scherer, A. Müller, and S. Behnke, in *International conference on artificial neural networks* (Springer, 2010), pp. 92–101.

[77] V. Nair and G. E. Hinton, in *Proceedings of the 27th international conference on machine learning (ICML-10)* (2010), pp.

807–814.

[78] D. P. Kingma and J. Ba, in *3rd International Conference on Learning Representations, ICLR 2015, San Diego, CA, USA, May 7-9, 2015, Conference Track Proceedings* (2015).

[79] G. E. Hinton, N. Srivastava, A. Krizhevsky, I. Sutskever, and R. R. Salakhutdinov, arXiv preprint arXiv:1207.0580 (2012).

[80] M. Abadi, P. Barham, J. Chen, Z. Chen, A. Davis, J. Dean, M. Devin, S. Ghemawat, G. Irving, M. Isard, et al., in *12th USENIX Symposium on Operating Systems Design and Implementation (OSDI 16)* (2016), pp. 265–283.

[81] We use the term ‘quasidistance’ since it does not respect triangular inequality. However, this fact plays no role as far as all the applications in the present paper are concerned.

Appendix A: Details on the architecture and on the training of the convolutional neural network

The first layer is a convolutional layer with 32 filters of size 2 by 2 and unit stride in both directions. Then the ‘max pooling’ [76] operation is applied with pool size 3 by 3, stride 2 in both directions and same padding. The results is then fully connected to a hidden layer with 100 neurons. The binary classification is finally done in the output softmax layer with two neurons. Both the convolutional and hidden fully connected layers are activated by rectified linear units (ReLU) [77]. The network is visualized in Fig. 5. We train the

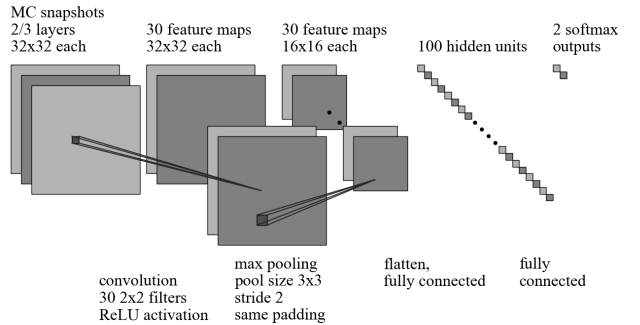


Figure 5: Visualization of the convolutional neural network used. Lower labels describe the layer operations. Upper labels describe the shapes of tensors before and after each operation.

network by minimizing the cross-entropy using the Adam [78] adaptive optimization algorithm with 7 epochs and minibatch size 25. Such choice leads to a fast training – the amount of training is much lower than in computer vision applications, routinely requiring hundreds or thousands of epochs – as well as prevention of overfitting by early stopping, hence eliminating the need for other measures such as dropout [79]. We use the following Adam algorithm parameters: learning rate 0.001 and standard choices of $\beta_1 = 0.9$ and $\beta_2 = 0.999$. We use Tensorflow [80] for the implementation.